11-1993

Reconstruction of Multiple Cracks from Experimental, Electrostatic Boundary Measurements

Kurt M. Bryan
Rose-Hulman Institute of Technology, bryan@rose-hulman.edu

Valdis Liepa
Rose-Hulman Institute of Technology

Michael Vogelius
Rose-Hulman Institute of Technology

RECONSTRUCTION OF MULTIPLE CRACKS FROM EXPERIMENTAL, ELECTROSTATIC BOUNDARY MEASUREMENTS

Kurt Bryan, Valdis Liepa and Michael Vogelius

MS TR 93-07

November 1993

Department of Mathematics
Rose-Hulman Institute of Technology
Terre Haute, IN 47803

FAX(812) 877-3198 Phone: (812) 877-8391

RECONSTRUCTION OF MULTIPLE CRACKS FROM EXPERIMENTAL, ELECTROSTATIC BOUNDARY MEASUREMENTS.

Kurt Bryan, Valdis Liepa and Michael Vogelius.

1 Introduction

The purpose of this presentation is to demonstrate the viability of using Electrical Impedance Tomography (EIT) for the reconstruction of multiple macroscopic cracks in a conductive medium. Through the use of EIT one seeks to determine the interior conductivity properties of a specimen from measurements of electrostatic potentials and currents on the boundary. There are obvious applications of this technology to many problems, for instance in medical tomography [5, 8] or nondestructrive testing of mechanical components [10]. There are two very separate classes of practical reconstruction techniques: 1) general imaging techniques, and 2) techniques that use prior information or assumptions. The first approach produces a somewhat blurry image of the conductivity distribution inside the specimen (somewhat akin to an ultrasound-scan) from which an "educated" user may then draw conclusions of a more specific nature (*cf.* [5, 8, 10, 18]). The second approach uses a restricted model for the interior conductivity distribution and seeks to determine more specific features within this model which are consistent with the measured data (*cf.* [13, 15, 16]). This may be done probabilistically, in a way reminiscent of methods for image reconstruction known as "maximum entropy methods" or deterministically by seeking to fit a relatively small number of parameters. In this presentation we shall concentrate on a very specific method of this last category. It seeks to determine a finite number of linear cracks consistent with the boundary measurements. In particular we shall test this algorithm on data which has been collected from laboratory experiments.

The mathematical results which insure a finite number of cracks can be reconstructed from a finite set of boundary voltages and boundary currents are found in [6, 11]. In these papers it is proven that n C^2 cracks inside a two dimensional domain may be determined from $n+1$ pairs of boundary voltages and boundary currents. These results have recently been extended to show that measurement of two pairs of boundary voltages and boundary currents suffice to determine any number of cracks [2, 9]. It is very easy to see that one measurement will not suffice to determine even a single crack, [11].

The computational algorithm we shall employ has largely been developed in [7]. It is the natural extension of an algorithm which was developed in [17] for the case of a single crack. We have modified the algorithm from [7] in one important respect, by making the selection of the initial guess automatic. For this purpose we have implemented some formulae which were suggested in [4] and which directly reconstruct the line on which a single linear crack must lie in order to be consistent with a single measurement of boundary voltage and boundary current. These formulae

may occasionally be degenerate, but the use of additional measurement pairs can eliminate this degeneracy.

An outline of this presentation is as follows. In section 2 we introduce the mathematical model used for simulating cracks and we give a brief discussion of our computational reconstruction method. In section 3 we present the formulae derived by Andrieux and Ben Abda and we briefly describe the selection of the initial crack. Section 4 contains a description of the experimental equipment used to collect the actual data for our reconstructions, and in particular we describe the few modifications that were made to the equipment used earlier to collect data for the reconstruction of a single crack [17]. In the fifth and final section we provide a number of examples of reconstructions of multiple cracks based on the collected experimental data.

2 The Mathematical Model and the Reconstruction Algorithm

A single crack inside a two dimensional conductor is commonly modeled as a perfectly insulating curve σ. With a background conductivity $0 < \gamma_0 \leq \gamma(x) \leq \gamma_1$ and a finite collection of cracks $\Sigma = \cup_{k=1}^{n} \sigma_k$, the steady state conductance equations thus read

$$\begin{aligned} \nabla \cdot (\gamma \nabla v) &= 0 \quad \text{in} \quad \Omega \setminus \Sigma, \\ \gamma \frac{\partial v}{\partial \nu} &= 0 \quad \text{on} \quad \Sigma, \end{aligned} \tag{2.1}$$

with appropriate boundary conditions on $\partial\Omega$, *e.g.*,

$$v = \phi \quad \text{on} \quad \partial\Omega. \tag{2.2}$$

The field ν is normal to Σ. The function v represents the potential induced in Ω. We assume that $\Omega \subset I\!R^2$ is simply connected, *i.e.*, has no holes, and so the entire boundary $\partial\Omega$ is accessible from the "outside". The domain Ω corresponding to our experimental data is a disk. Let u denote the "γ-harmonic" conjugate to v. It is related to v by the formula

$$(\nabla u)^{\perp} = \gamma \nabla v \ \text{ in } \ \Omega \setminus \Sigma, \tag{2.3}$$

where $\perp$ indicates counterclockwise rotation by $\pi/2$. Note that the set $\Omega \setminus \Sigma$ is not simply connected; the existence of a "γ-harmonic" conjugate u owes not only to the fact that $\nabla \cdot (\gamma \nabla v) = 0$ in $\Omega \setminus \Sigma$, but also to the fact that $\gamma \frac{\partial v}{\partial \nu} = 0$ on Σ. For a particular set of constants c_k, $k = 1, \ \ldots \ , n$, the function u solves the problem

$$\begin{aligned} \nabla \cdot (\gamma^{-1} \nabla u) &= 0 \quad \text{in} \quad \Omega \setminus \Sigma, \\ u &= c_k \quad \text{on} \quad \sigma_k, \ k = 1, \ \ldots \ , n \end{aligned} \tag{2.4}$$

with

$$\gamma^{-1} \frac{\partial u}{\partial \nu} = \psi = \frac{\partial \phi}{\partial s} \ \text{ on } \ \partial\Omega. \tag{2.5}$$

Here s denotes the counterclockwise tangent direction on $\partial\Omega$ and ν denotes the outward normal on $\partial\Omega$. For these particular constants, finding a solution to (2.4)-(2.5) is thus equivalent to finding a solution to (2.1)-(2.2) . The constants c_k may (up to a common additive constant) be characterized

in several equivalent ways (see [7]). The characterization we shall use here takes the form of the system of n equations

$$\int_{\sigma_k} [\gamma^{-1} \frac{\partial u}{\partial \nu}] \, ds = 0, \quad 1 \leq k \leq n. \tag{2.6}$$

Here $[\gamma^{-1} \frac{\partial u}{\partial \nu}] = \gamma^{-1} \frac{\partial u}{\partial \nu_+} - \gamma^{-1} \frac{\partial u}{\partial \nu_-}$ denotes the jump in the normal flux across the curve σ_k. [1] The system (2.6) should be viewed as a supplement to the boundary value problem (2.4)-(2.5). The solution u has a physical interpretation in its own right – it is the potential generated by the boundary current ψ for a medium with background conductivity γ^{-1} and a set of perfectly conducting cracks σ_k, $k = 1, \ldots, n$. As follows immediately from the relation (2.3), on passes between the boundary data corresponding to v and that corresponding to u by differentiating the Dirichlet-data along the boundary, integrating the Neumann-data along the boundary and interchanging the roles of the two. Except when we explicitly say so we shall always work with cracks that are perfectly conducting in the sense described above. Let $P_1, \ldots, P_M$ and $Q_1, \ldots, Q_M$ be $2M$ points on $\partial\Omega$. For the crack reconstruction we utilize solutions corresponding to the two-electrode currents $\psi_j = \delta_{P_j} - \delta_{Q_j}$, $j = 1, \ldots, M$,

$$\begin{aligned} \nabla \cdot (\gamma^{-1} \nabla u_j) &= 0 \quad \text{in} \quad \Omega \setminus \Sigma, \\ u_j &= c_k^{(j)} \quad \text{on} \quad \sigma_k, \; k = 1, \ldots, n, \end{aligned} \tag{2.7}$$

with

$$\gamma^{-1} \frac{\partial u_j}{\partial \nu} = \delta_{P_j} - \delta_{Q_j} \quad \text{on} \quad \partial\Omega, \tag{2.8}$$

the constants $c_k^{(j)}$ being determined through the additional equations (2.6). The reconstruction problem may now be stated explicitly as follows:

We seek to reconstruct the collection of cracks $\Sigma = \cup_{k=1}^n \sigma_k$ *from knowledge of the boundary voltage data* $\{u_j|_{\partial\Omega}\}_{j=1}^M$ *corresponding to the prescribed two-electrode currents* $\gamma^{-1} \frac{\partial u_j}{\partial \nu} = \delta_{P_j} - \delta_{Q_j}$, $j = 1, \ldots, M$.

It was shown in [6] that if we take $M = n + 1$, $Q_1 = Q_2 \ldots = Q_{n+1} = P_0$ and we take P_j, $1 \leq j \leq n + 1$ to be mutually different and different from P_0, then the boundary voltage measurements corresponding to the resulting $n + 1$ fixed two-electrode currents $\delta_{P_j} - \delta_{P_0}$, $1 \leq j \leq n + 1$ suffice to uniquely identify a collection of n (or fewer) cracks. By a clever extension of this analysis it has recently been shown that two fixed two-electrode currents suffice to uniquely identify any number of cracks, [2, 9]. It is very easy to see (*cf.* [11]) that measurements corresponding to a single boundary current does not suffice to determine even a single crack. In the papers [6, 11] it was required that the reference conductivity γ be real analytic. This requirement has recently been considerably relaxed; the identifiability result holds even if γ is only Hölder continuous [9].

A certain amount of knowledge is available concerning continuous dependence. In the case in which the background conductivity is constant and there is at most only one crack present it has been shown (*cf.* [1]) that if the boundary voltage data (on some open subset of $\partial\Omega$) deviate by ϵ, then the crack locations differ by at most $[\log(|\log \epsilon|)]^{-1/4}$. If the single crack is linear it has been shown that the crack location depends Lipschitz continuously on the boundary data, [3]. This last

[1] The expression $\frac{\partial u}{\partial \nu_+}$ denotes the limit of the derivative (in the direction ν) as one approaches σ_k from the side to which ν points. $\frac{\partial u}{\partial \nu_-}$ denotes the limit as one approaches σ_k from the opposite side.

result significantly extends a calculation found in [11], showing that transverse translations and rotations of a single linear crack depend Lipschitz continuously on the measured data.

As mentioned before, we shall in the present reconstructions always try to fit the data by means of linear cracks. We shall also assume that the background conductivity may be modeled by a constant, *e.g.*, $\gamma \equiv 1$. As was the case in [17], we base the reconstruction of the cracks on the values of a relatively small number of functionals (as opposed to all the boundary measurements). In [17] we used 4 functionals corresponding to the reconstruction of a single linear crack, here we use $4n$ functionals for the reconstruction of n cracks. We now give a brief description of these functionals. For more details we refer the reader to [7, 17].

Let $\mathbf{F}$ denote the vector-valued function

$$\mathbf{F}(\Sigma, \psi, \mathbf{w}) = (F(\Sigma, \psi, w^{(1)}), F(\Sigma, \psi, w^{(2)}), F(\Sigma, \psi, w^{(3)}), F(\Sigma, \psi, w^{(4)}))^t,$$

where $F(\Sigma, \psi, w)$ is given by

$$F(\Sigma, \psi, w) = \int_{\partial\Omega} u(\Sigma, \psi) \frac{\partial w}{\partial \nu}\, ds, \tag{2.9}$$

and where $w^{(i)}$, $1 \leq i \leq 4$, are particular solutions of

$$\Delta w = 0 \quad \text{in} \quad I\!R^2 \setminus \Sigma.$$

The function $u = u(\Sigma, \psi)$ is the solution to (2.4)-(2.5) with $\gamma \equiv 1$. In order to make u unique we may for instance impose the requirement

$$\int_{\partial\Omega} u\, ds = 0 \ . \tag{2.10}$$

The appropriate selection of boundary currents ψ and test functions $\mathbf{w} = (w^{(1)}, w^{(2)}, w^{(3)}, w^{(4)})^t$ is very important and was discussed in detail in [7]. For our reconstruction algorithm we always choose ψ in the form of a two-electrode current. We take one ψ and one $\mathbf{w}$ corresponding to each crack σ_k; whenever we want to emphasize this correspondence we use the notation

$$\psi_{\sigma_k} \quad \text{and} \quad \mathbf{w}_{\sigma_k} = (w^{(1)}_{\sigma_k}, w^{(2)}_{\sigma_k}, w^{(3)}_{\sigma_k}, w^{(4)}_{\sigma_k})^t.$$

We shall always take $\mathbf{w}$ so that

$$\int_{\partial\Omega} \frac{\partial w^{(i)}}{\partial \nu}\, ds = 0, \quad \text{and} \quad \int_{\sigma} \left[\frac{\partial w^{(i)}}{\partial \nu}\right] ds = 0 \ \ \forall \sigma \in \Sigma. \tag{2.11}$$

Because of the first identity in (2.11) the function $\mathbf{F}$ is unchanged by the addition of a constant to u, and we can therefore work with any other normalization in place of (2.10). The data for our reconstruction consist of measured boundary potentials. In practice we can of course only measure the values of these potentials at a finite (fairly moderate) number of points. We denote by $g(\psi)$ the voltage data corresponding to the boundary current ψ, and we define a corresponding vector-valued function

$$\mathbf{f}\,(\psi, \mathbf{w}) = (f(\psi, w^{(1)}), f(\psi, w^{(2)}), f(\psi, w^{(3)}), f(\psi, w^{(4)}))^t,$$

where $f(\psi, w)$ is given by

$$f(\psi, w) = \int_{\partial\Omega} g(\psi) \frac{\partial w}{\partial \nu}\, ds, \tag{2.12}$$

and where $w^{(i)}$ are the same functions as before. Our algorithm seeks a solution $\Sigma = \{\sigma_k\}_{k=1}^n$ to the $4n$ equations

$$\mathbf{F}(\Sigma, \psi_{\sigma_k}, \mathbf{w}_{\sigma_k}) = \mathbf{f}\,(\psi_{\sigma_k}, \mathbf{w}_{\sigma_k}), \quad 1 \leq k \leq n. \tag{2.13}$$

We do not use information about the full set of measured boundary voltages for the reconstruction; we only use information about the values of these particular functionals. This is in contrast to the reconstructions from experimental data which we presented in [13], and where we used all the measured boundary voltages and a least squares approach. Based on extensive experimentation it is our experience that almost all the relevant information is contained in these functionals. Admission of the extra data, *e.g.* after convergence of the algorithm based on the functionals, does not generally seem to improve the reconstructions. In several examples in which we tried the least squares approach from the start it actually impeded the convergence process, due to the presence of local minima, we think.

The construction of the test functions $w^{(i)}$ is quite simple to describe. If we consider a single linear crack, and use a coordinate system so that the crack lies on the x-axis (the line of reals) then the functions $w^{(1)}$ and $w^{(2)}$ are given by

$$w^{(1)} = Im[z], \quad w^{(2)} = Im[z^2]\,.$$

The functions $w^{(3)}$ and $w^{(4)}$ have square-root singularities at the endpoints of the crack; if the crack lies between the origin and the point $(\lambda, 0)$ they have the form

$$w^{(3)} = \begin{cases} Re[(z-\lambda)\sqrt{z(z-\lambda)}], & Re(z) > \frac{\lambda}{2} \\ -Re[(z-\lambda)\sqrt{z(z-\lambda)}], & Re(z) < \frac{\lambda}{2}\,, \end{cases} \tag{2.14}$$

$$w^{(4)} = \begin{cases} Re[\sqrt{z(z-\lambda)}], & Re(z) > \frac{\lambda}{2} \\ -Re[\sqrt{z(z-\lambda)}], & Re(z) < \frac{\lambda}{2}\,. \end{cases} \tag{2.15}$$

Intuitively $w^{(1)}$ and $w^{(2)}$ detect transverse translations and rotations of the crack, whereas $w^{(3)}$ and $w^{(4)}$ detect translations along the direction of the crack and variations in length. It is interesting to note that in the limit as λ approaches zero the information extracted by these four functions approach the first four nontrivial Fourier modes of the boundary data. We refer the reader to [7]for more details.

The selection of the applied currents is also fairly simple to describe: for a single crack we select the location of the two electrodes in a way which maximizes the sensitivity of the four functionals with respect to rotations and transverse translations of the crack. We use an iterative approach to solve (2.13), in this case for the single crack σ. At each step new electrode locations are found by maximizing two of the diagonal elements of the Jacobian of $D_\sigma \mathbf{F}$ with respect to the boundary electrode locations (taking the fixed test functions described above). Measured data corresponding to these electrode locations are then used to find an updated crack. The selection procedure is described in detail in [7, 17]. When the domain is a disk, and the crack is of moderate size and sits away from the boundary, then the most sensitive electrode locations defined above turn out (very nearly) to be the points that arise as the intersection of the line on which the crack lies and the domain boundary (remember, the crack is perfectly conducting). Our selection of electrodes does

require the solution of an auxiliary boundary value problem. However, as explained later, this is done very efficiently through an integral equation formulation. For the reconstruction of more than one crack we select a boundary current corresponding to each crack, as if the other cracks were not present. This process is described in detail in [7].

The $4n \times 4n$ system (2.13) is solved by means of a Newton method. As explained above, the test functions and the applied currents change with each step of the iteration. The update for each step of the Newton method is constrained, along the lines of the classical Levenberg-Marquardt approach [14].

The boundary value problems which must necessarily be solved in order to evaluate F (and find the "optimally sensitive" electrode locations) are formulated in terms of boundary integral equations. The system of boundary integral equations is a mixture of first and second kind equations. There is a first kind contribution corresponding to the functions that describe the normal derivative "jumps" on each crack. However, by working with the boundary condition u =constant on each crack, we avoid the problem associated with non-integrable kernels. We discretize the integral equations by Nyström's method, as completely described in [7]. The kernels of the first kind contributions are singular enough that we did not find it necessary to regularize the equations. Also, we note that we do not really numerically compute the $u|_{\partial\Omega}$ necessary to evaluate F, rather we compute $(u-u_0)|_{\partial\Omega}$, where u_0 is the potential generated by the exact same electrode locations and currents as u, but without any cracks present. The computation of the smooth function $(u-u_0)|_{\partial\Omega}$ is a much better posed problem than the computation of $u|_{\partial\Omega}$. Because the domain Ω is a disk, the function u_0 has a very simple explicit expression. Whenever necessary we add its values to the computed differences.

3 Apparatus and Data Collection

In this section we give a brief description of the apparatus with which we collected the experimental data used to test the crack reconstruction algorithm. Most of these details can also be found in [13]; nonetheless, for the convenience of the reader we will recount them here.

The reconstruction algorithm is designed for a two dimensional region with a constant background conductivity. An experimental equivalent is given by the tank illustrated in Figure 1. The tank is cylindrical and constructed of 0.25 inch thick plexiglass, with an inside diameter of 10.5 inches and a height of 23.5 inches. The tank is filled with distilled water to which a small amount of ordinary tap water is added, which gives the solution a modest electrical conductivity. Twelve evenly spaced copper electrodes run vertically along the full height of the tank. The copper electrodes are 0.25 inches wide. Since the entire apparatus is uniform in the vertical direction, and since the electrodes are essentially perfectly conducting (in relation to the interior solution), the tank provides a reasonable approximation to a two-dimensional electrical conduction problem. To introduce perfectly conducting "cracks" we insert strips of sheet metal with widths ranging from 2 to 6 inches vertically into the tank, again preserving the uniformity of the conduction problem in the vertical direction. A grid is placed under the tank (which has a plexiglass bottom) so that the location of the cracks can be easily recorded.

The overall structure of the data collection apparatus is as follows. Each electrode is attached to a binding post on the top rim of the tank. These binding posts are connected, through a bank

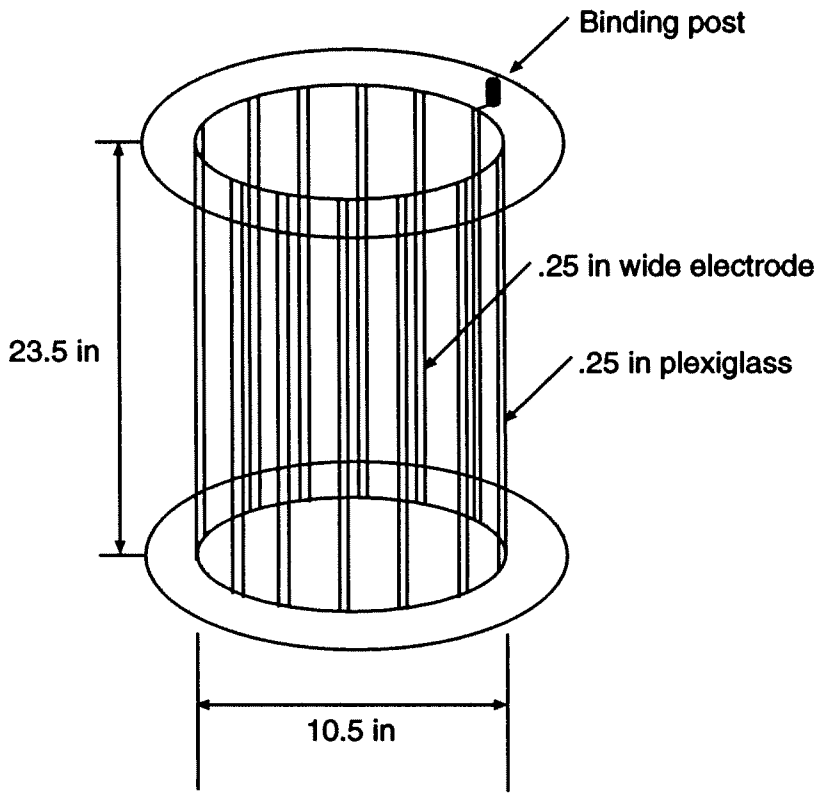

Figure 1: Tank used for data collection.

of relay cards, to a current source and a pair of digital multimeters. One multimeter serves to measure the electrical current supplied to the tank when a specified pair of electrodes is active. The other multimeter measures the induced voltage drop between any given pair of electrodes. By altering the electrical connections via the relay cards, any pair of electrodes can act as the source and sink for the electrical current and the voltmeter can measure the resulting potential across any two electrodes. The entire apparatus is connected to a PC which controls the relay cards, allowing software switching of the active electrodes and voltage measurements. The PC and software also communicate with the multimeters, collect the resulting current and voltage information, and present it in a convenient format. A simple schematic of the entire apparatus is given in Figure 2.

As mentioned in [13], while the problem is modeled as a steady-state or DC conduction problem, in practice one uses AC currents. This is to avoid any electrochemical plating of the electrodes with the impurities present in the water, which might alter the behavior of the electrodes, particularly the contact resistance between the electrodes and water. We use a sinusoidal source with a frequency of 1 kHz, which should be low enough to be considered steady-state so that no phase changing capacitance or inductance effects will be significant. In actuality, a few experiments were conducted with frequencies from 10 Hz to 1 kHz without any cracks in the tank, and in this range no frequency dependent effects were observed.

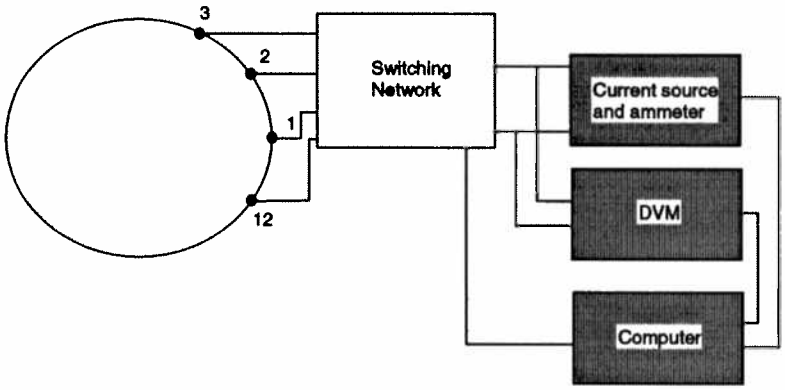

Figure 2: Schematic of data collection system.

The data collection software is written in BASIC. As discussed in the previous section, at the heart of the crack recovery algorithm is the idea of iteratively adapting the active electrode locations for greater sensitivity as the algorithm progresses and more precise information about the actual crack location(s) becomes available. However, since the reconstruction algorithm could not immediately be ported to the PC which collects the data, it was necessary to collect all possible data a priori. When the reconstruction algorithm was later run using this data set (on a separate computer), it simply extracted the required voltage data corresponding to the desired active electrode locations. One can easily check that for a tank with 12 electrodes there are only 11 different linearly independent combinations of input and output electrodes; the solution corresponding to any other current pattern can be represented as a linear combination of the solutions corresponding to these basic current patterns. In its dipole current pattern mode the software collects data for the current patterns $\psi_j = \delta_{j+1} - \delta_j$, $j = 1, \ldots, 11$, that is, a current is introduced at electrode $j+1$ and withdrawn at electrode j. Whenever the recovery algorithm needs a different current pattern during its execution it simply takes an appropriate linear combination of the data corresponding to these 11 basic patterns.

For the data sets which will be presented, typical values for the input current were 4 to 7 mA (rms). Typical voltage drops between electrodes range from zero to 7 volts rms, with the largest drops between the active input and output electrode. The previous version of the software, used to collect the data in [13], recorded the input current to only 2 significant figures. In the course of taking measurements for this paper it was observed that even the third significant figure for the current was quite consistent and stable from measurement to measurement. The software was thus modified to record three significant figures for the input current. As before, voltages are recorded to four figures. An application of the crack reconstruction algorithm to both types of data (two versus three significant figures for current measurement) indicate that the latter is considerably more accurate. It appears that for this experimental setup, the crack manifests much information concerning its presence and location in this third significant digit, particularly for multiple crack problems.

Before proceeding with the reconstruction algorithm one must also know k, the background conductivity of the tank. To obtain this information we applied the current patterns $\psi_1, \ldots, \psi_{11}$ described above to the tank with no cracks and measured the corresponding induced voltages. We then used the same current patterns in our computational model and computed the corresponding

theoretical voltage. These voltages scale linearly with $\frac{1}{k}$, and so one can easily compute that value for k which gives the best fit of the computational model to the measured voltages, in the sense of mean square error. Doing this yielded an average resistivity of 456.6 ohms, or a conductivity of 0.00219 mhos. This value varied by only %1 over the course of the tests (approximately 30 different crack configurations over 2 days). This is the value of k which was used in all crack reconstructions. In practice we scaled the measured data by k so that it formally corresponds to a background conductivity of one. All our subsequent computations were then done with a conductivity of 1.

One final remark is in order. The electrodes on the actual tank have a necessarily non-zero width, while the simple theoretical model we use assumes point electrodes. This assumption leads to logarithmic singularities in the theoretical voltage at the current input and output electrodes. Moreover, in the actual experimental data any contact resistance between the electrode surface and the water leads to inaccuracies in the voltage measurements at the active electrodes, since Ohm's law implies that if a current is flowing through the electrode and a resistance is present, there must be a voltage drop across the electrode. Thus the voltage on the tank side of the active electrode (the voltage required by the algorithm) may differ from the voltage measured by the multimeter which is on the other "side" of the contact resistance. This is not a problem for voltage measurements at non-active electrodes; these electrodes have essentially no current flowing (the multimeter presents an input impedance of $> 10^9$ ohms), hence no voltage drop. We thus omit from consideration the voltages at active electrodes for both the experimental and computational data. One merely adjusts the numerical integration rule for computing the functionals $F(\Sigma, \psi, w^{(i)})$ to account for the gap.

While a more accurate model incorporating a non-zero width electrode could certainly be derived and the algorithm adapted to deal with such a model, the agreement between the measured data and theoretical computations was so good that there seemed little to be gained by refining the model, at least for cracks which are not extremely close to an active electrode.

4 A Simple Formula for the Line of a Single Crack

In [4] two very simple formulae are given for reconstructing the line on which a single linear, perfectly insulating crack lies. These formulae are in terms of a single voltage/current pair measured on the boundary of Ω. The formulae are restricted to the reconstruction of a single line. As has already been observed, a single crack (even a linear one) is not uniquely identifiable from a single measurement. As far as these explicit formulae are concerned this expresses itself in terms of the possibility of the vanishing of a certain denominator (more about this later). The formulae do not require the solution of any boundary value problems, but only the evaluation of certain weighted integrals of the voltage and current data on the boundary of the region. These formulae merely locate the line on which the crack lies, they do not tell us where on the line the crack is. It is possible to determine the exact location of the crack by evaluating an infinite number of similar integrals and reconstructing the support of a function from its Fourier series (see [4]). We have not implemented this latter step as part of our algorithm, but we have incorporated the simple formulae for the reconstruction of a single line as part of the initialization step of our crack reconstruction algorithm. Once the line is found, the initial guess is chosen to be centered on that segment of the

line which lies inside the domain (a disk). In the reconstructions we present later the initial guess is, rather arbitrarily, taken to be of length $0.1\times$ the radius of the disk.

We now briefly review the formulae from [4]. Suppose that σ is a perfectly insulating linear crack in Ω and $v(x)$ is a function on $\Omega \subset I\!R^2$ which satisfies

$$\begin{aligned} \Delta v &= 0 \quad \text{in} \quad \Omega \setminus \sigma \\ \frac{\partial v}{\partial \nu} &= 0 \quad \text{on} \quad \sigma \,, \end{aligned}$$

where ν is a unit normal vector field on σ. Note that this field is constant since σ is linear. Based on the boundary values of v and $\frac{\partial v}{\partial \nu}$ on $\partial\Omega$ we can then recover the line $\nu \cdot x = c$ on which the crack σ lies as follows. Let $\phi_i(x)$ denote any of the two coordinate functions $\phi_i(x) = x_i$. Note that ϕ_i are both harmonic. Define the quantities I_i, $i = 1, 2$, by

$$I_i = \int_{\partial\Omega} \left(v \frac{\partial \phi_i}{\partial \nu} - \phi_i \frac{\partial v}{\partial \nu} \right) ds, \quad \phi_i(x) = x_i. \tag{4.16}$$

These quantities depend only on boundary values of v and its normal derivative, and can be easily computed from the known data, e.g., when $\frac{\partial v}{\partial \nu}$ is specified (a current applied) and v is measured on $\partial\Omega$, or vice-versa. Let $[v]$ denote the jump in u across σ; $[v]$ is defined as $v_+ - v_-$, where v_+ denotes the values of v as one approaches σ from the side to which the fixed normal field ν points, and v_- denotes the values as one approaches from the opposite side. A simple application of the divergence theorem shows that

$$I_i = \int_\sigma [v] \frac{\partial \phi_i}{\partial \nu} \, ds \,,$$

since $\frac{\partial v}{\partial \nu}$ vanishes on σ. Now note that $\frac{\partial \phi_i}{\partial \nu} \equiv \nu_i$ on σ, since $\phi_i = x_i$. Thus

$$I_i = \nu_i \int_\sigma [v] \, ds \,. \tag{4.17}$$

If we assume $\int_\sigma [v] \, ds \neq 0$ it then follows that

$$\left(\int_\sigma [v] \, ds \right)^2 = I_1^2 + I_2^2 \,,$$

and

$$\nu_i = \pm I_i / \sqrt{I_1^2 + I_2^2} \,.$$

This gives us a normal vector to the line on which σ lies. To be precise let us choose ν corresponding to the $+$ sign, *i.e.*,

$$\nu_i = I_i / \sqrt{I_1^2 + I_2^2} \,. \tag{4.18}$$

From (4.17) it follows that

$$\int_\sigma [v] \, ds > 0$$

for this choice of ν, and therefore

$$\int_\sigma [v] \, ds = \sqrt{I_1^2 + I_2^2} \,.$$

We now recover the constant c, of the equation $\nu \cdot x = c$ for the line on which σ lies. Let us rotate our coordinate system so that the normal vector ν to σ has coordinates $(0, 1)$. Since we know ν this

rotation is known; the line on which σ lies is still $\nu \cdot x = c$, or simply $x_2 = c$. Let $\phi(x) = \frac{1}{2}(x_2^2 - x_1^2)$ in this new coordinate system. The function $\phi(x)$ is again harmonic. Define I_ϕ by

$$I_\phi = \int_{\partial\Omega} \left(v \frac{\partial \phi}{\partial \nu} - \phi \frac{\partial v}{\partial \nu} \right) ds \ . \tag{4.19}$$

Application of the divergence theorem shows that

$$I_\phi = \int_\sigma [v] \frac{\partial \phi}{\partial \nu} \, ds \ .$$

Since $\nabla \phi = (-x_1, x_2)$ and since $\nu = (0, 1)$, this becomes

$$I_\phi = \int_\sigma [v] x_2 \, ds \ ,$$

or

$$I_\phi = c \int_\sigma [v] \, ds \ ,$$

so that

$$c = I_\phi / (\int_\sigma [v] \, ds) = I_\phi / \sqrt{I_1^2 + I_2^2} \ ,$$

again assuming that the denominator does not vanish. This formula in combination with the formulae (4.16) and (4.18) gives a simple way of determining the line on which a single linear, perfectly insulating crack lies.

We cannot generally take for granted that $\int_\sigma [v] \, ds$ is non-zero, given a single fixed boundary current $\frac{\partial v}{\partial \nu}$ on $\partial\Omega$. This is certainly the generic case, but it is not difficult to see that a single applied boundary current can not guarantee that this is true for all σ. This is consistent with the general result [11] that one needs two applied currents and corresponding voltage measurements even to find a single crack. If the applied currents are all two-electrode currents it is very easy to see that a finite number will suffice in order to obtain $I_1^2 + I_2^2 \neq 0$ for any interior crack for at least one of these currents . By a more detailed analysis it is possible to show that any two different two-electrode currents always suffice [2].

We note that the choices for the three auxiliary functions used for reconstructing the line on which the crack lies are harmonic polynomials of degree ≤ 2, quite similar to the weight functions used in our crack reconstruction algorithm. In the limit (as crack length goes to zero) our four weight functions $\omega^{(1)}$ through $\omega^{(4)}$ span the space of harmonic polynomials of degree ≤ 2, modulo constants. This is also the reason why in the case of a disk the limiting information contained in the functionals is equivalent to the first 4 nontrivial Fourier modes, as noted earlier.

Finally let us note that it is very easy write the quantities I_i and I_ϕ in terms of data corresponding to the harmonic conjugate to v, *i.e.*, in terms of data corresponding to a perfectly conducting σ. Given a smooth function f on $\partial\Omega$ which satisfies $\int_{\partial\Omega} f ds = 0$ let $\int^s f$ denote a counterclockwise integral of f along $\partial\Omega$, *i.e.*, a function whose counterclockwise tangential derivative equals f. From the relation 2.3 with $\gamma = 1$ we now immediately obtain

$$I_\phi = \int_{\partial\Omega} \left(v \frac{\partial \phi}{\partial \nu} - \phi \frac{\partial v}{\partial \nu} \right) ds = \int_{\partial\Omega} \left(-\frac{\partial u}{\partial \nu} (\int^s \frac{\partial \phi}{\partial \nu}) - \frac{\partial \phi}{\partial \tau} u \right) ds$$

where $\frac{\partial}{\partial \tau}$ denotes the counterclockwise tangential derivative on $\partial\Omega$. Similar formulae for I_i are obtained by replacing ϕ with ϕ_i. We use these formulae directly instead of making any transformations to our measured boundary data.

5 Reconstruction Experiments

We have performed numerous experiments with the equipment described in section 3 followed by reconstructions using the algorithm described in section 2. In this section we discuss the results in three different scenarios, that we find to be representative. In the first scenario two flat metal strips were inserted in the tank to simulate perfectly conducting cracks. We varied the locations of the two metal strips inside the tank in order to give some idea of how the information contents of the measured data deteriorates as the cracks lie deeper and deeper inside the domain. In the second scenario three flat metal strips were inserted to demonstrate that the data does indeed permit one to distinguish more than one or two cracks. We have not at the moment experimented with a number of cracks larger than three, partially because of the practical difficulties associated with the accurate insertion of a large number of cracks, but also because we feel it is likely that the currently available accuracy of the data (and the mathematical model) will make such reconstructions extremely crude. In the third scenario we used a single metal strip, but this time bent so that its cross section forms an L-shape. This experiment demonstrates that the collected data has sufficient information content to distinguish a shape which differs from a line segment, and it also demonstrates the flexibility of the reconstruction algorithm to approximate such a shape. In our opinion the results presented here clearly demonstrate the viability of impedance imaging as a method to reconstruct a moderate number of macroscopic cracks from experimental data.

Let us give a brief description of the figures. Each figure depicts two disks to illustrate one iteration of the reconstruction algorithm. The location of the reconstructed crack(s) are indicated by solid lines. Those in the disk to the left are the locations prior to the particular iteration, and those in the disk on the right are the locations after the iteration is complete. The dashed lines in the disk to the right indicate the locations of the true cracks as read off from the mesh at the bottom of the tank. The "optimally sensitive" electrode locations that were used for this iteration are indicated on the boundary of the disk to the left. We select one pair of optimally sensitive electrodes corresponding to each crack, according to the strategy briefly described earlier in section 2; n cracks will thus correspond to 2n active electrode locations. This is in contrast to [7], where we also selected one pair of electrodes corresponding to each crack but fixed one electrode location to be shared by all the electrode pairs; in those reconstructions n cracks corresponded to $n+1$ active electrode locations. We found that in the presence of the "noisy" experimental data the reconstructions were improved by not forcing one common electrode. Although we have not indicated on the figures which electrode pair corresponds to which crack, it is almost evident, given the observation we made earlier concerning a single perfectly conducting crack. The optimally sensitive electrodes are located near the intersection of the boundary and the line on which the crack lies. Figure 3a shows the first iteration using experimental data corresponding to two cracks, but in this case the algorithm seeks to reconstruct only a single crack. The initial guess shown in the disk to the left lies on the line generated by the formulae of Andrieux and Ben Abda. We have chosen the initial guess to be of length .1×the radius of the disk, and to be centered on that segment of the line which lies inside the disk. Figure 3b shows the fifth iteration of the algorithm when starting with the initial guess shown in Figure 3a. At this point the algorithm has converged in the sense that the maximum of all four components of G is less than 10^{-10} in absolute value. We now take this crack and divide it into two pieces by omitting a central piece, 1/10 of the cracks size. The resulting two cracks are given as initial data to our algorithm. After 83 iterations the reconstructed cracks have converged to the two cracks shown in the right disk of

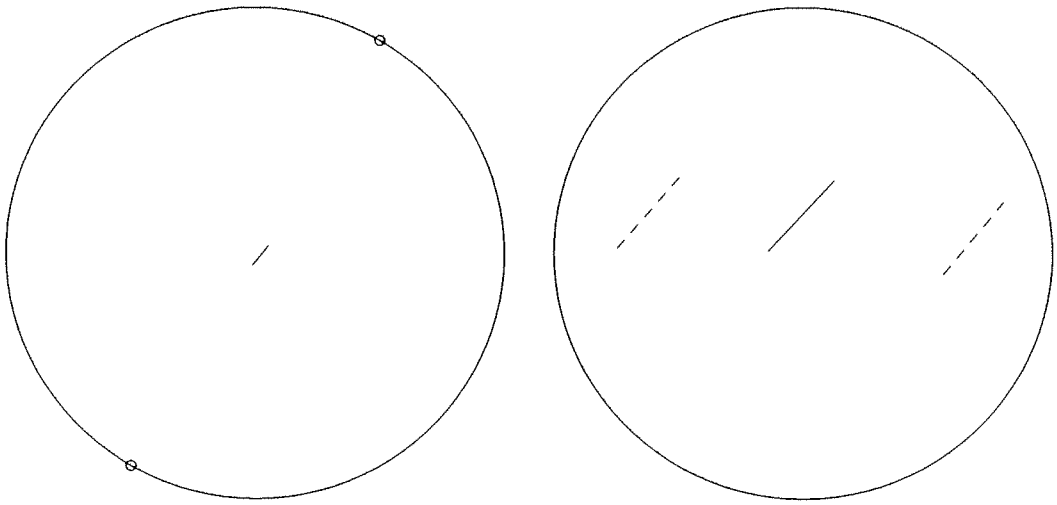

Figure 3a

The first iteration reconstructing one crack. The "true" crack locations are shown in dashed lines in the disk to the right. The currently active electrode locations are indicated on the circle to the left.

Figure 3c. We have run several examples with data originating from two cracks. As one would expect the reconstructed cracks deviate more from the true cracks when the true cracks are closer to the center of the disk. The above reconstruction is quite representative of cracks located about 1/3 of the way towards the center. Figures 4a and 4b show the iterations at which convergence is reached when reconstructing one and two cracks respectively, given data that correspond to two true cracks located about halfway towards the center. Figures 5a and 5b show reconstructions obtained from data corresponding to two true cracks located approximate 3/4 of the way towards the center. Figure 5a shows the fifth iteration reconstructing only a single crack, at which point this process has converged. We divide the resulting crack into two pieces by cutting out a central piece 1/10 of its size, and feed these two cracks as initial guess to our algorithm reconstructing two cracks. Figure 5b shows the 50th iteration of the two-crack reconstruction process. There is no convergence, nor does any converged state appear to be reached at a later iteration (we have run the process to 100 iterations with basically the same result). The collected data is apparently not accurate enough to distinguish these two cracks from a single crack near the center. We now proceed with a scenario involving three "true" cracks. We start by reconstructing one crack which,in the sense of our functionals, is consistent with the data. The initial guess is generated by means of the Andrieux-Ben Abda formulae, as described earlier. We take the converged crack as shown in Figure 6a (after 6 iterations), divide it into two pieces and feed the resulting cracks as an initial guess to our algorithm for the reconstruction of two cracks. After convergence (in this case after another 33 iterations, as shown in Figure 6b) we divide the largest of the reconstructed cracks into two pieces, and feed the 3 resulting cracks as an initial guess to our algorithm for the reconstruction of three cracks. Figure 6c shows the results of the three-crack reconstruction after 50 iterations. Convergence has not been attained, but notice that the reconstructed cracks seem to give a reasonable prediction of locations. It almost goes without saying that the prediction of the

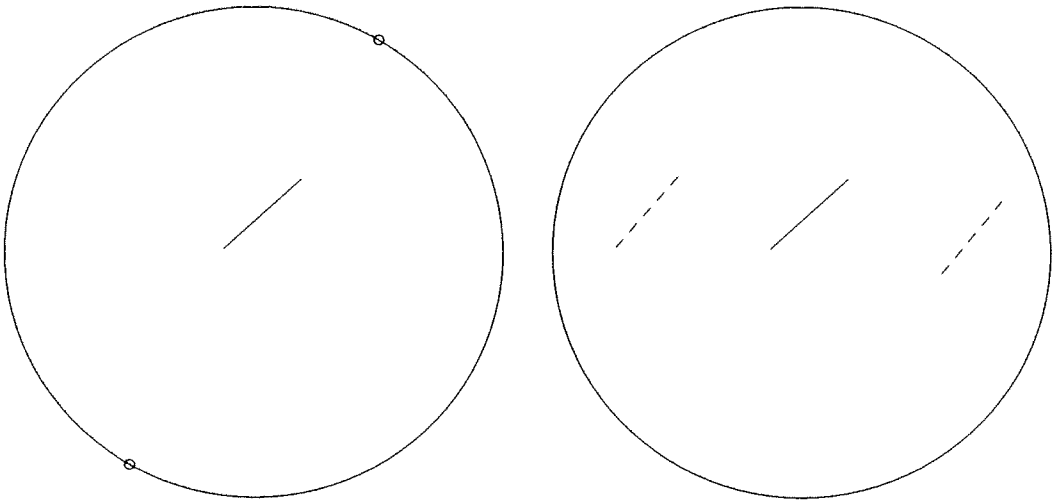

Figure 3b

The 5th iteration reconstructing one crack. The collected data are the same as in Figure 3a. The "true" crack locations are shown in dashed lines in the disk to the right. The currently active electrode locations are indicated on the circle to the left.

length of one of the cracks is considerably off.

Finally, in Figures 7a and 7b we show the converged reconstructions using one and two cracks respectively and data which come from insertion of a single strip of metal which has been bent so that its cross section forms an L-shape.

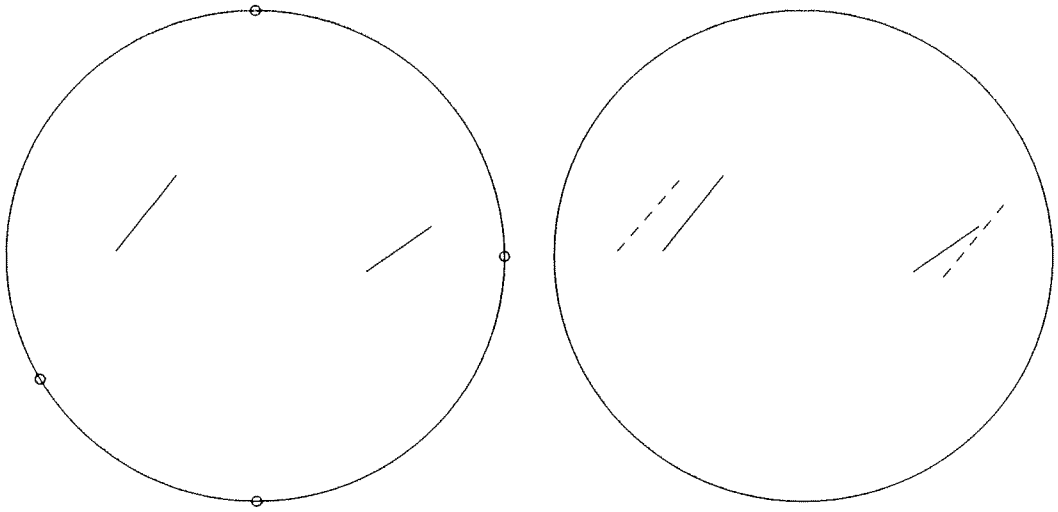

Figure 3c

The 83rd iteration reconstructing two cracks. The collected data are the same as in Figures 3a and 3b. The "true" crack locations are shown in dashed lines in the disk to the right. The currently active electrode locations are indicated on the circle to the left.

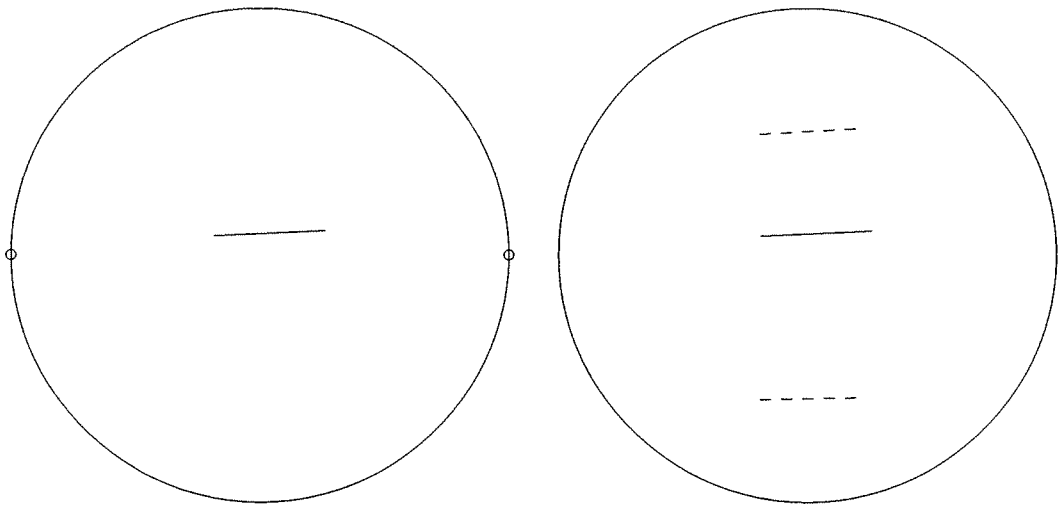

Figure 4a

The 6th iteration reconstructing one crack. The "true" crack locations are shown in dashed lines in the disk to the right. The currently active electrode locations are indicated on the circle to the left.

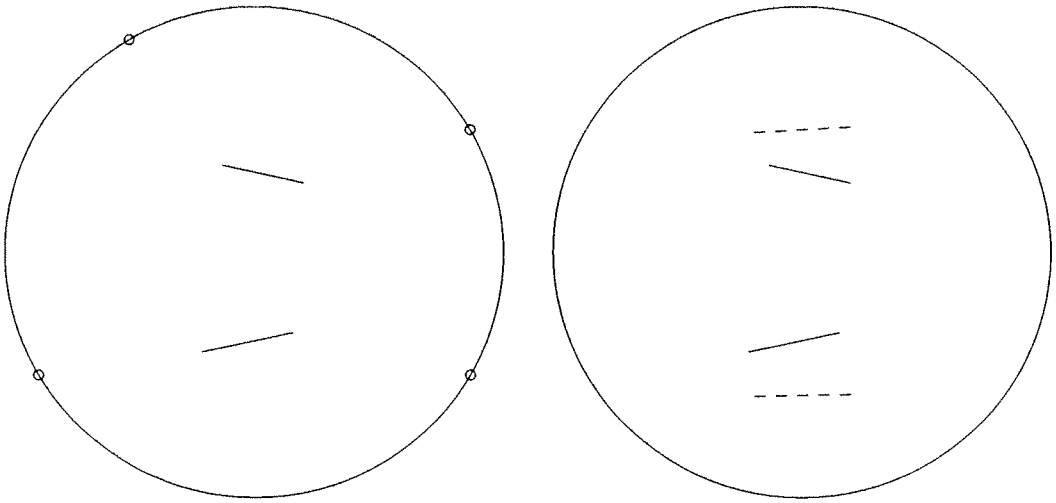

Figure 4b

The 31st iteration reconstructing two cracks. The collected data are the same as in Figure 4a. The "true" crack locations are shown in dashed lines in the disk to the right. The currently active electrode locations are indicated on the circle to the left.

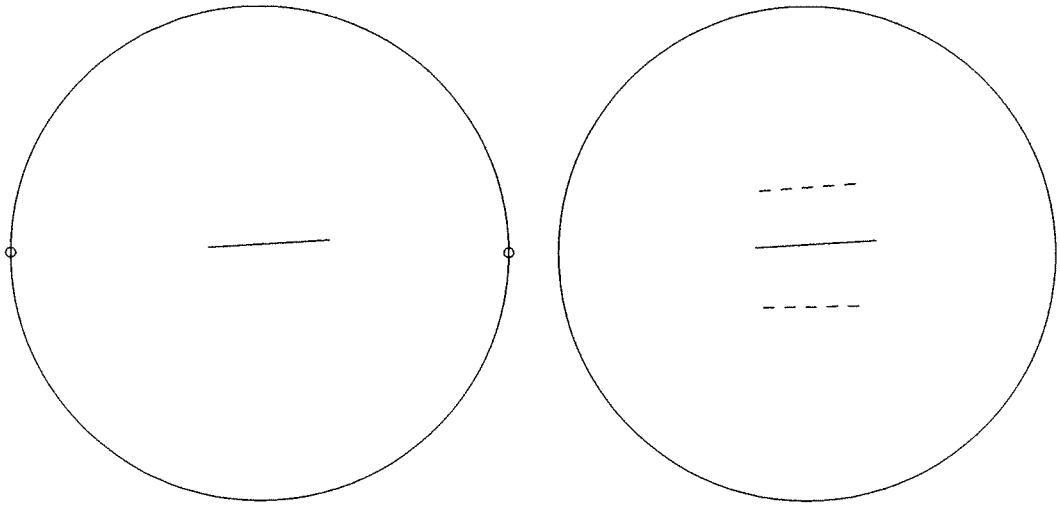

Figure 5a

The 5th iteration reconstructing one crack. The "true" crack locations are shown in dashed lines in the disk to the right. The currently active electrode locations are indicated on the circle to the left.

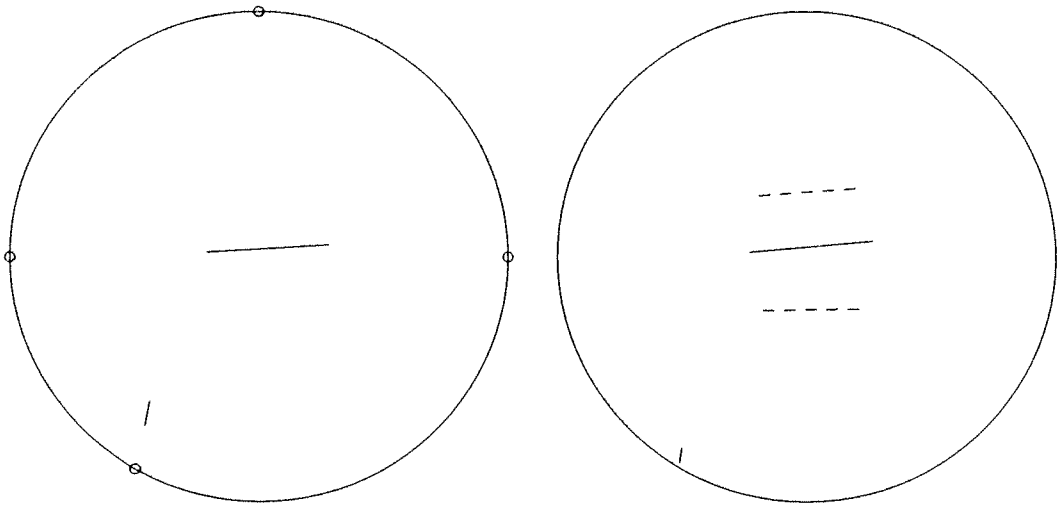

Figure 5b

The 50th iteration reconstructing two cracks. The collected data are the same as in Figure 5a. Convergence has not been reached. The "true" crack locations are shown in dashed lines in the disk to the right. The currently active electrode locations are indicated on the circle to the left.

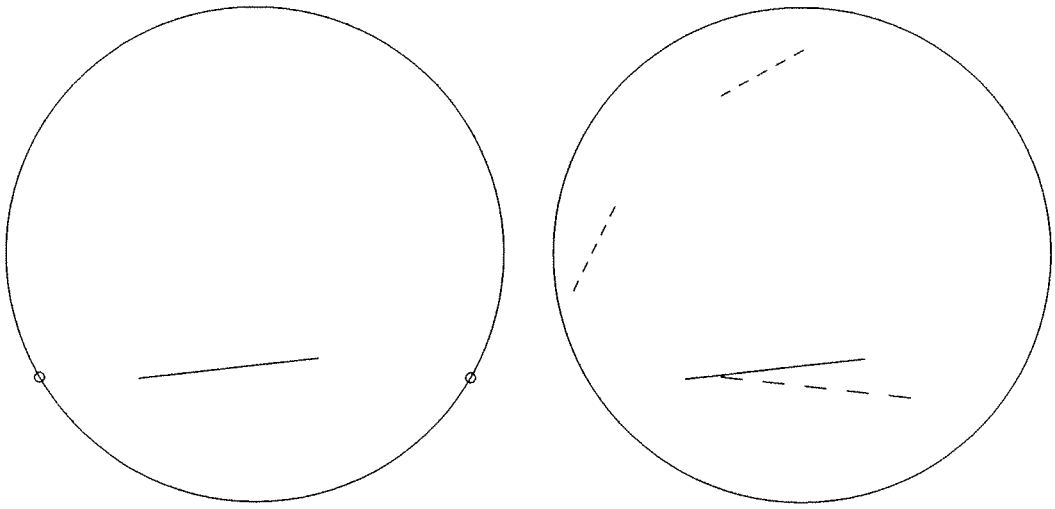

Figure 6a

The 6th iteration reconstructing one crack. The "true" crack locations are shown in dashed lines in the disk to the right. The currently active electrode locations are indicated on the circle to the left.

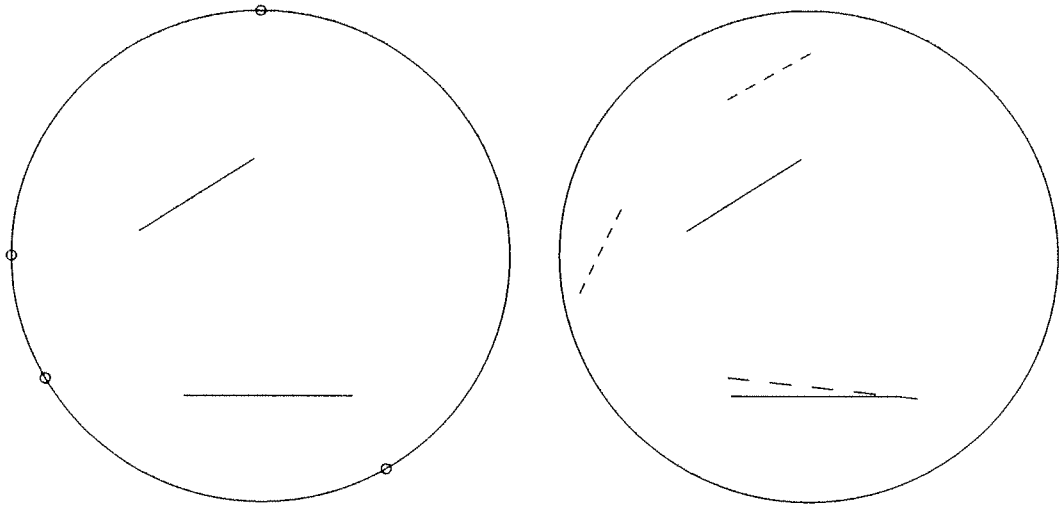

Figure 6b

The 33rd iteration reconstructing two cracks. The collected data are the same as in Figure 6a. The "true" crack locations are shown in dashed lines in the disk to the right. The currently active electrode locations are indicated on the circle to the left.

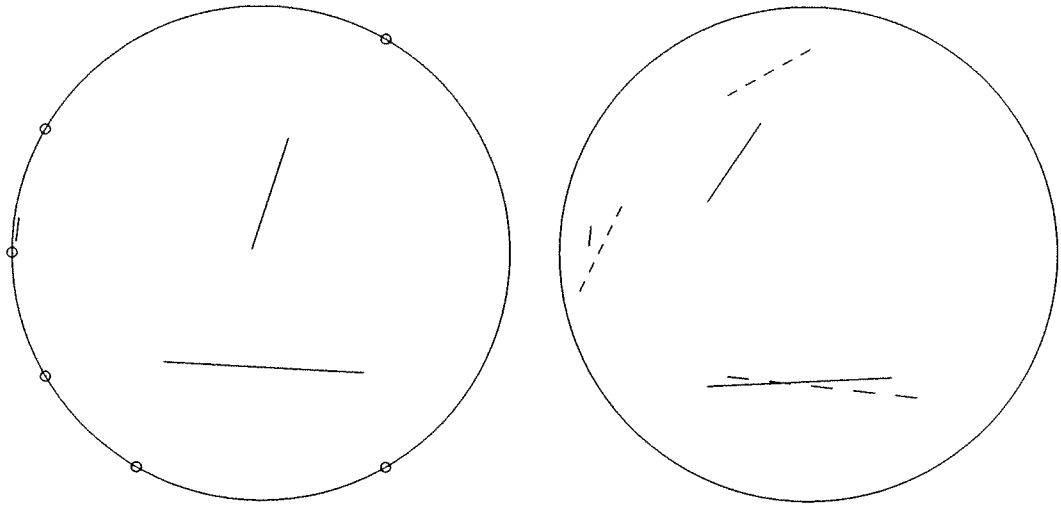

Figure 6c

The 50th iteration reconstructing three cracks. The collected data are the same as in Figures 6a and 6b. Convergence has not been reached. The "true" crack locations are shown in dashed lines in the disk to the right. The currently active electrode locations are indicated on the circle to the left.

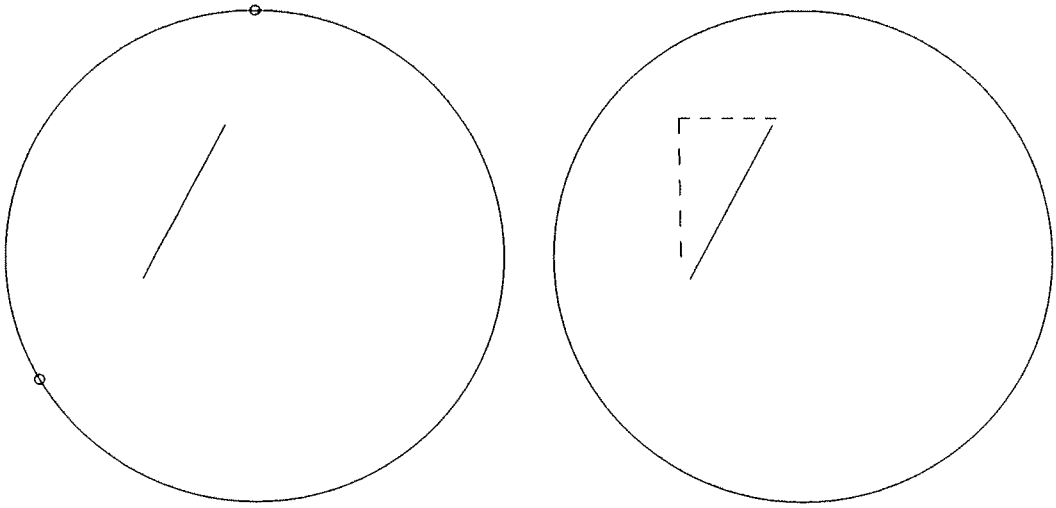

Figure 7a

The 7th iteration reconstructing one crack. The "true" crack location is shown as a dashed curve in the disk to the right. The currently active electrode locations are indicated on the circle to the left.

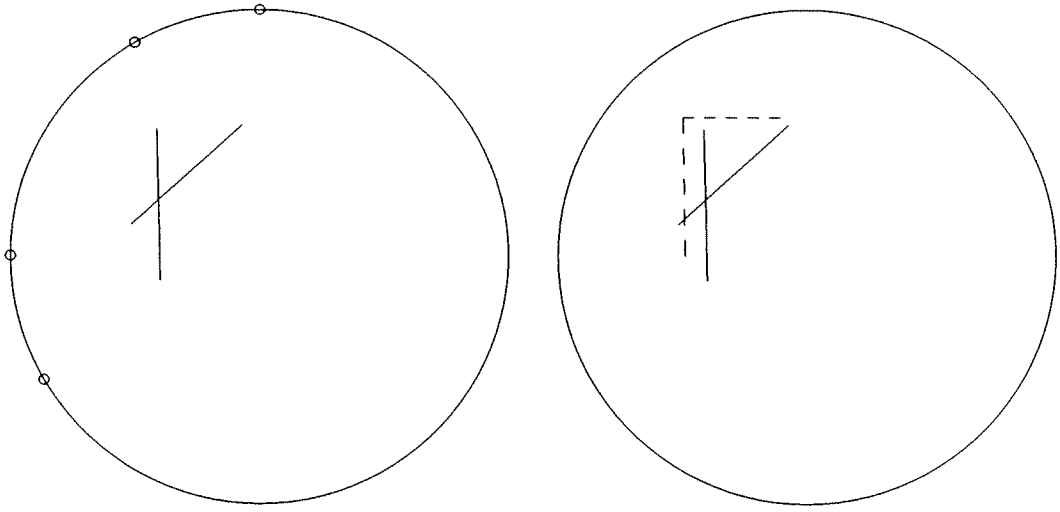

Figure 7b

The 12th iteration reconstructing two cracks. The collected data are the same as in Figure 7a. The "true" crack location is shown as a dashed curve in the disk to the right. The currently active electrode locations are indicated on the circle to the left.

Acknowledgments

This research was partially supported by NSF grant DMS-9202042, AFOSR contract 89NM605, and NASA contract NAS1-19480. This work was performed while the third author was visiting the Université Joseph Fourier during the academic year 92/93. He would like to thank his colleagues at "Laboratoire de Modelisation et Calcul" for the hospitality extended to him and in particular Jacques Blum for his efforts towards making this visit possible.

This work was performed while the first author was in residence at the Institute for Computer Applications in Science and Engineering at NASA Langley Research Center, Hampton, VA.

References

[1] Alessandrini, G., Stable determination of a crack from boundary measurements. To appear, Proc. Roy. Soc. Edinburgh.

[2] Alessandrini, G., Personal communication.

[3] Alessandrini, G., Beretta, E. and Vessella, S., Determining linear cracks by boundary measurements – Lipschitz stability. Preprint, 1993.

[4] Andrieux, S. and Ben Abda, A., Identification de fissures planes par une donnée de bord unique: un procédé direct de localisation et d'identification. C. R. Acad. Sci. Paris, Serié I, 315 (1992).

[5] Barber, D. and Brown, B., Recent developments in applied potential tomography - APT, in Information Processing in Medical Imaging, Bacharach, S. ed., Nijhoff, Amsterdam, 1986, pp. 106–121.

[6] Bryan, K. and Vogelius, M., A uniqueness result concerning the identification of a collection of cracks from finitely many electrostatic boundary measurements. SIAM J. Math. Anal., 23 (1992), pp. 950–958.

[7] Bryan, K. and Vogelius, M., A computational algorithm to determine crack locations from electrostatic boundary measurements. The case of multiple cracks. To appear in Int. J. Engng. Sci.

[8] Cheney, M., Isaacson, D., Newell, J., Simske, S. and Goble, J., NOSER: An algorithm for solving the inverse conductivity problem, Int. J. Imaging Systems and Tech., 22 (1990), pp. 66–75.

[9] Diaz Valenzuela, A. Unicità et stabilità per il problema inverso del crack perfettamente isolante. Thesis, University of Trieste, 1993.

[10] Eggleston, M.R., Schwabe, R.J., Isaacson, D., Goble, J.C. and Coffin, L.F., Three-dimensional defect imaging with electric current computed tomography. GE Technical Report 91CRD039, Schenectady, NY.

[11] Friedman, A. and Vogelius, M., Determining cracks by boundary measurements. Indiana Univ. Math. J., 38 (1989), pp. 527–556.

[12] Gisser, D.G., Isaacson, D. and Newell, J.C., Electric current computed tomography and eigenvalues. SIAM J. Appl. Math., 50 (1990), pp. 1623–1634.

[13] Liepa, V., Santosa, F. and Vogelius, M. Crack determination from boundary measurements. Computational reconstruction from laboratory measurements. Technical report 92-12, Center for the Mathematics of Waves, University of Delaware. Submitted to Journal of Nondestructive Evaluation.

[14] Moré, J., The Levenberg-Marquardt algorithm: implementation and theory. *Numerical Analysis* (Edited by Watson, G.A.), pp. 105–116. *Lecture Notes in Math.* 630. Springer Verlag, 1977.

[15] Nishimura, N., Regularized integral equations for crack shape determination problems. *Inverse Problems in Engineering Sciences* (Edited by Yamaguti, M. et al), pp. 59–65. Springer Verlag, 1991.

[16] Nishimura, N. and Kobayashi, S., A boundary integral equation method for an inverse problem related to crack detection. Int. J. Num. Meth. Eng., 32 (1991), pp. 1371–1387.

[17] Santosa, F. and Vogelius, M., A computational algorithm to determine cracks from electrostatic boundary measurements. Int. J. Eng. Sci. 29 (1991), pp. 917–937.

[18] Yorkey, T., Webster, J. and Tompkins, W., Comparing reconstruction algorithms for electrical impedance tomography. IEEE Trans. Biomedical Eng., BME-34 (1987), pp. 843–852.

Department of Mathematics
Rose-Hulman Institute of Technology
Terre Haute, IN 47803

Radiation Laboratory, Dept EECS
University of Michigan
Ann Arbor, MI 48109

Department of Mathematics
Rutgers University
New Brunswick, N.J. 08903